NUREG/CR-6672: RESPONSE OF GENERIC CASKS TO COLLISIONS

Douglas J. Ammerman
Sandia National Laboratories*
Albuquerque, New Mexico, 87185-0718, USA 505/845-8158

ABSTRACT

This paper describes the calculations performed to determine the response of four generic spent fuel casks to impact accidents that support the generic risk assessment of NUREG/CR-6672 [1]. The generic casks analyzed represent the most typical types of casks currently used in the United States to transport spent fuel: truck casks with steel-lead-steel and steel-DU-steel walls and rail casks with steel-lead-steel and monolithic steel walls. The specifications for these casks are discussed in another paper of this symposium [2]. This paper discusses the results from finite element calculations for impacts onto a rigid target in three orientations and at four velocities for the generic monolithic steel rail cask. These calculations are unique in that they modeled the entire cask, including closure bolts, and failure was directly measured by calculation of the degree of opening in the closure.

In a risk assessment, as well as in the real world, most collisions do not involve impact onto a rigid target. In order to account for the energy absorbed by the target, an energy partitioning scheme was used to develop impact speeds onto yielding targets that were equivalent to the impact speeds onto the rigid target considered in the analyses. The frequency distribution of various targets is discussed in a companion paper [3].

In the transport of spent nuclear fuel, the containment boundary of the cask is not the only barrier to release. The cladding of the fuel can also provide containment. This paper also discusses the method used to determine the response of the cladding to the analyzed impacts. Knowing the response of the fuel and the response of the cask to various impacts allows rod-to-cask and cask-to-environment release fractions to be calculated. The calculations of these parameters are given in a companion paper [3].

FINITE ELEMENT CALCULATIONS FOR IMPACTS ONTO RIGID TARGETS

To determine the response of the generic casks, finite element calculations for impacts onto rigid targets were conducted. For all of the analyses in this paper, the Sandia-developed non-linear transient dynamics finite element program PRONTO-3D [4, 5, 6] was used to determine the damage resulting from each impact. For each generic cask, calculations were performed for impacts in end-on, CG-over-corner, and side-on orientations. All impacts are assumed to be onto a flat, rigid surface with the initial cask velocity perpendicular to the surface. While it is possible for a cask to impact a surface that is not flat (such as a bridge column) in a side impact orientation (such that the contact occurs between the impact limiters), this type of accident was not considered. An impact of this type only provides loading and, therefore, deformation to the cylindrical portion of the cask body away from the closure area. This part of the cask is

* Sandia is a multiprogram laboratory operated by Sandia Corporation, a Lockheed Martin Company, for the United States Department of Energy under Contract DE-AC04-94AL85000.

extremely ductile, and can withstand deformations greater than the cask diameter without causing the cask to leak.

To shorten the analysis times and avoid calculation of the very large shear strains that occur in the impact limiter, at the start of all of the analyses, it was assumed that the impact limiter has already been driven into the lock-up region (the point at which the material stops crushing). Using the pre-crushed impact limiter, analyses with impact velocities of 30, 60, 90, and 120 mph were conducted for each cask and orientation. If the energy required to crush the impact limiters is added to the initial kinetic energy of the cask, these analysis velocities correspond to actual impact velocities of 42, 67, 95, and 124 mph.

While it is possible to create a finite element mesh that accurately models all of the details of the generic cask models, using meshes of this size requires too much computation time for the many cases considered in this work. For this reason, simplifying assumptions were made. All of the impacts considered have a plane of symmetry through the long axis of the cask, so it is only necessary to model one-half of the structure. Figure 1 shows the finite element model used for the lead shielded rail cask, typical of the models used for all of these analyses.

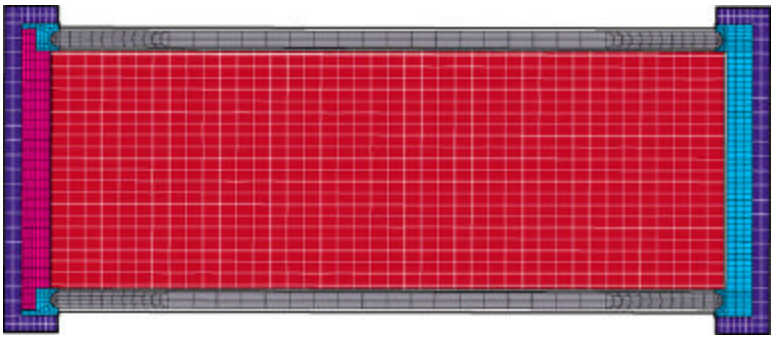

Figure 1 - Finite element model of the steel-lead-steel rail cask.

For all of the sandwich-wall casks, the inner and outer steel layers were modeled with zero-thickness shell elements. This type of element accurately captures the bending behavior and axial forces in the shell, but does not incorporate stresses in the direction perpendicular to the shell surface.

The behavior of the neutron shielding and its liner has little effect on deformations in the ends and body of the cask, and if modeled would slightly reduce this damage. For this reason, these components were not modeled, but rather their mass was lumped with the mass of the contents to achieve the correct package weight. The cask contents and basket were treated as a homogenous crushable material. The crush strength of this material was chosen from the buckling strength of PWR fuel pins subjected to axial loads. Because the only purpose of the contents within the model is to provide loading onto the cask, variations in their material properties has little effect on the analysis results.

For all of the analyses, the initial velocity vector of the cask was assumed to be perpendicular to the rigid target surface. All of the interior contact surfaces in the model (between the contents and the inner shell, the gamma shielding and both shells, the lid and the cask body, and the cask body and the impact limiter)

were assumed to be frictionless. The contact between the cask and the rigid surface was also frictionless. For most aspects of the problem, this assumption is conservative, as there is no loss of impact energy because of frictional heating. Including friction at contact surfaces tends to cause the various parts of the modeled structure to behave more like a single piece (decreases separation of the parts of the structure being modeled). Neglect of friction and the orientation assumed for the initial velocity guarantee that the displacement, velocity, and acceleration vectors will always be in a direction that is perpendicular to the rigid surface.

The closure of the cask is explicitly modeled. The lid is recessed into the body of the cask and held in place with either 12 (6 in the half-symmetric model) 1-inch diameter bolts for the truck casks or 24 (12 in the half-symmetric model) 1.75-inch diameter bolts for the rail casks. The bolt model cross-section is square with square heads. The area of the square bolt shank is the same as the area of a real round bolt. The edges of the heads are rigidly attached to the cask lid, and the bottom of the shank is rigidly attached to the cask body. Figure 2 shows the cross-section through the center of a typical bolt and an isometric view of a single bolt. All of the contacts are tied via coincident nodes.

The O-ring grooves and O-rings for the seals are not included in the model, but the deformations in the sealing surfaces at the locations of the O-rings are tracked to determine when the opening exceeds the compliance of the O-ring resulting in failure of the seal. For the O-rings typical of spent fuel casks there should be no leakage for openings up to 0.100 inches.

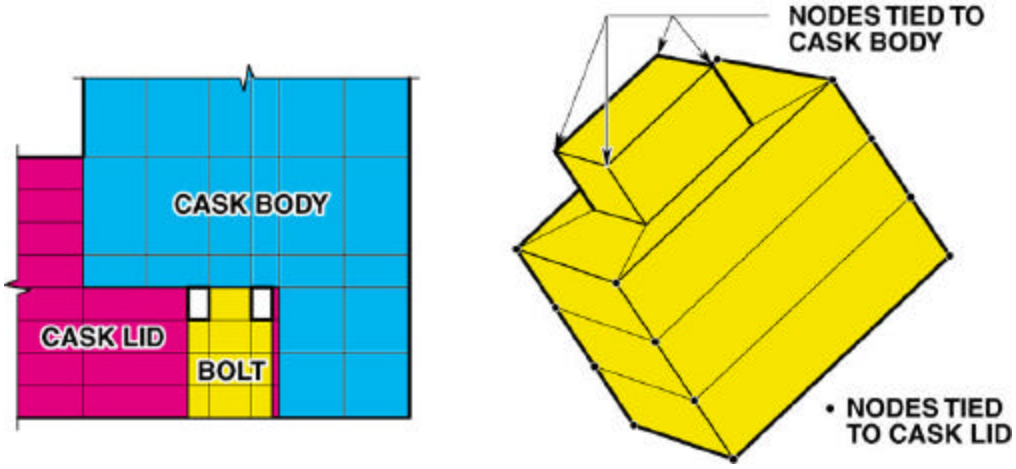

Figure 2 - Typical model of a bolt used in the finite element analyses.

Using finite element analyses to determine the ability of the casks to maintain containment requires investigation of all of the factors that may result in a loss of containment. For these casks the main factors to consider are maximum tensile plastic strains in the containment boundary, maximum tensile plastic strains in the closure bolts, and deformations in the region of the seals. For the monolithic rail cask the maximum strain on the interior surface of the cask is less than 60 percent for all analyses. The maximum occurs at the lid-cask interface for the 120-mph side impact case. At this location most of the plasticity is caused by compression, so there is no possibility of material failure. Table 1 lists the maximum strains on the inside of this cask for these analyses.

Table 1 - Maximum Plastic Strains on the Inside of the Monolithic Rail Cask

Corner Impact		End Impact		Side Impact	
Speed	**Strain (%)**	**Speed**	**Strain (%)**	**Speed**	**Strain (%)**
30 mph	< 10	30 mph	< 2	30 mph	< 10
60 mph	< 20	60 mph	< 5	60 mph	< 30
90 mph	< 30	90 mph	< 10	90 mph	< 50
120 mph	< 50	120 mph	< 17	120 mph	< 60

The chance of a closure failure is directly related to the deformations between the cask lid and cask body and tensile or shear failure of the bolts. For the conservative bolt model used in these analyses, the maximum strain in any of the bolts for each impact speed is shown in Table 2. Several of these analyses indicate bolt strains that are high enough that failure of the bolt is likely (strains greater than 50 percent are assumed to cause failure because the bolt material has a specified percent elongation greater than 15 percent and a specified percent reduction of area greater than 50 percent [7] which correlates to a true strain at failure of 69 percent). A value of 50 percent is conservatively chosen to indicate bolt failure because the material model used for the bolts has the true stress in the bolts equal to the ultimate tensile stress (an engineering stress) at a strain of 50 percent. Limiting the bolt stress to the ultimate tensile stress also assures that the bolt threads will not fail. Bolt true strains that are higher than 50 percent are shown in **bold** in the table. Several other analyses indicate bolt strains that are high enough for failure of the bolts to be possible (true strains higher than 25 percent). These bolt strains are shown in *italics* in the table.

Table 2 - Maximum True Strain in the Closure Bolts for the Monolithic Steel Rail Cask

Corner Impact		End Impact		Side Impact	
Speed	**Strain (%)**	**Speed**	**Strain (%)**	**Speed**	**Strain (%)**
30 mph	14	30 mph	4	30 mph	15
60 mph	*40*	60 mph	14	*60 mph*	*32*
90 mph	**67**	*90 mph*	*35*	**90 mph**	**104**
120 mph	**80**	**120 mph**	**58**	**120 mph**	**170**

The amount of deformation between the cask body and the lid at the location of the O-ring seals determines if a leak path from the cask is generated. Because the seal grooves were not explicitly included in the model, the deformation at a location that is near where the O-rings would be located is used. For each model the displacement of two sets (upper point and lower point) of two nodes on the cask lid and one node on the cask body are tracked for all times. Initially these three nodes are co-linear, with the body node lying between the two lid nodes. From the displacement time histories, the amount of seal separation and seal sliding can be determined. The seal separation is defined as the movement of the body node that is normal to the line between the two lid nodes. The sliding is defined as the movement of the body node along the line between the two lid nodes. Figure 3 shows these displacements for the 90-mph end impact of the monolithic steel rail cask. Table 3 shows the seal region displacements at the end of the finite element analyses.

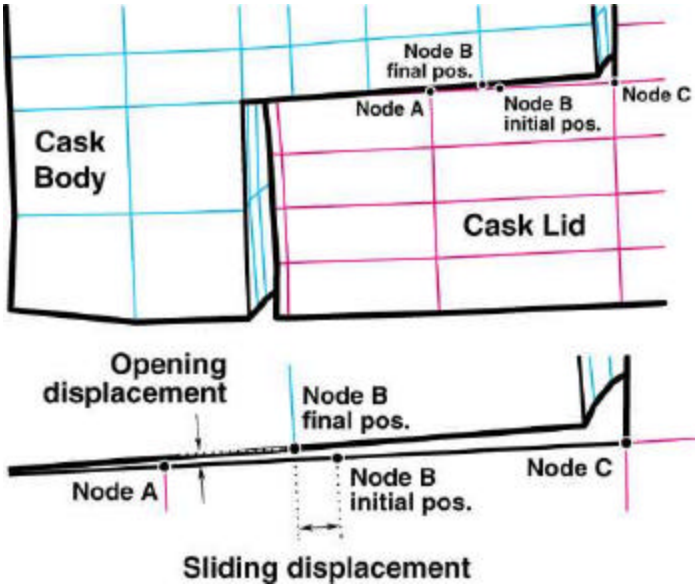

Figure 3 - Seal region displacements for the 90-mph end impact of the monolithic steel rail cask.

Table 3 - Seal Closure Displacements, in Inches, at the End of the Analysis

Analysis Velocity	Corner Impact		End Impact		Side Impact	
	Opening	Sliding	Opening	Sliding	Opening	Sliding
30 mph	0.04	0.20	0.007-0.053	0.04-0.05	0.01	0.01
60 mph	0.10	0.36	0.04-0.12	0.09-0.10	0.04	0.01
90 mph	0.22	0.48	0.03-0.13	0.38-0.39	0.08	0.09
120 mph	0.44	0.59	0.09-0.16	0.668	0.12	-

To determine the leak area that results from these opening displacements, the influence of the pre-compression of the elastomeric O-ring and the width of the opening must be considered. For cases with maximum openings of less than 0.100 inches, the pre-compression of the O-ring (as much as 0.112 inches for 3/8-inch O-rings and 0.150 inches for 1/2-inch O-rings at 30 percent compression for static face seal configurations [8]) will allow it to recover sufficiently to maintain sealing and thus prevent release of radioactive material. For opening displacements between 0.100 and 0.200 inches, the difference in bolt strains indicates that the opening only occurs at the location of one bolt. The width of the leak path is then equal to the bolt spacing (6.38 inches for the rail casks). However, for part of this width, the actual opening displacement will be less than the O-ring compression; therefore, the area of the resulting hole is calculated by truncating the base (the truncated part has a height of 0.100 inches) of an isosceles triangle with a height of the opening displacement and a width of the bolt spacing. For opening displacements between 0.200 and 0.300 inches, the opening occurs over two bolt spacings, and for opening displacements greater than 0.300 inches, it is assumed the opening occurs over three bolt spacings. For opening displacements greater than 0.300 inches, the resulting leak area is sufficiently large that increasing

the width of the opening has little or no effect on the amount of release. Table 4 summarizes the leak path calculations for the analyses where the maximum closure opening is greater than 0.100 inches.

Table 4 - Calculated Monolithic Steel Rail Cask Closure Leak Path Areas

Velocity (mph)	Orientation	Opening Displacement (inches)	Opening Width (inches)	Leak Path Area (in^2)
60	Corner	0.103	6.38	0.00028
90	Corner	0.216	12.76	0.40
120	Corner	0.439	19.14	2.5
120	Side	0.123	6.38	0.014

IMPACTS ONTO REAL TARGETS

The finite element results discussed in the previous section are all for impacts onto a rigid target. For this type of impact, the entire kinetic energy of the impact is absorbed by the cask. For finite element analyses, a rigid target is easily implemented by enforcing a no displacement boundary condition at the target surface. In real life, the construction of a rigid target is impossible, but it is possible to construct a target that is sufficiently rigid that increasing its rigidity does not increase the amount of damage to the cask. This is because in real impacts there is a sharing of energy absorption between the cask and the target. If the target is much weaker than the cask, the target will absorb most of the energy. If the target is much stronger than the cask, most of the energy will be absorbed by the cask. The partitioning of the impact energy between the cask and several "real-world" targets was developed in order to obtain impact speeds onto real surfaces that cause the same damage as the modeled impacts onto rigid targets. Impacts onto hard desert soil and concrete highways are discussed below.

For each finite element calculation of impact onto a rigid target, the total kinetic energy of the finite element model is output at 100 time-steps through the analysis. The total kinetic energy is one half of the sum of the mass associated with each node times the velocity of that node squared. From the time-history of kinetic energy, a velocity time history is derived. The rigid-body velocity for each time-step is calculated assuming that all of the kinetic energy of the model is caused by velocity in the direction of the impact.

Numerical differentiation of the velocity time-history gives the rigid-body acceleration. The contact force between the rigid target and the cask at any time is assumed to be equal to the rigid-body acceleration times the mass of the cask. Using this, a force time-history can be generated for each impact analysis.

For each analysis the peak contact force is determined. Table 5 lists these forces. For an impact onto a real yielding target to be as damaging to the cask as the modeled impact onto the rigid target, the yielding target must be able to impart a force equal to this peak force to the cask.

The energy absorbed by the target in developing this force is added to the initial kinetic energy of the cask. This total absorbed energy is used to calculate an equivalent velocity.

Table 5 - Peak Contact Force from Impacts Onto Rigid Targets for the Monolithic Steel Rail Cask (Pounds)

Corner Impact		End Impact		Side Impact	
30 mph	2.1E7	30 mph	3.8E7	30 mph	2.2E7
60 mph	3.9E7	60 mph	9.5E7	60 mph	5.4E7
90 mph	5.8E7	90 mph	1.1E8	90 mph	9.5E7
120 mph	7.5E7	120 mph	1.3E8	120 mph	1.1E8

The force deflection curves for various targets were derived from results of impact tests performed by Gonzales [9], Waddoups [10], and Bonzon and Schamaun [11] and from engineering principles. Integration of the force-deflection curve up to the peak contact force determines the amount of energy absorbed by the target.

The concrete targets resist penetration by two modes, generation of a failure zone in the concrete and subsequent penetration into the subgrade. The force required to generate the failure zone in the concrete, and the energy absorbed in creating it, depends on the impact velocity, the size of the impacting cask, and the thickness of the concrete. The additional penetration is governed by the same behavior as penetration into soil targets.

The results for the monolithic steel rail cask are given in Table 6.

Table 6 - Real Target Equivalent Velocities (mph) for the Monolithic Steel Rail Cask

Target/Orientation		Rigid Target Velocity			
		30 mph w/o limiter	60 mph w/o limiter	90 mph w/o limiter	120 mph w/o limiter
Soil	End	>150	>>150	>>150	>>150
	Side	92	>150	>>150	>>150
	Corner	111	>150	>>150	>>150
Concrete Slab	End	>150	>>150	>>150	>>150
	Side	104	>>150	>>150	>>150
	Corner	>>150	>>150	>>150	>>150

FAILURE OF RODS

The percentage of fuel pins failed for each impact is estimated from the peak rigid-body acceleration. The STACE report [12] provides strains in the fuel pin cladding for a 100-G side impact for both PWR and BWR assemblies. Table 7 gives the maximum strain in each rod. In that report, it was shown that side impact provides the most severe loading to the fuel assemblies. In this report, the maximum strain generated in a fuel rod due to impacts onto a rigid target at any of the four speeds and three impact orientations modeled by the finite element calculations were estimated using the peak acceleration of the impact to scale the largest strain generated in a fuel rod

Table 7 - Peak Strains in Fuel Rods Resulting from a 100 G Impact

Fraction of PWR Rods	Peak Strain (%)
1/15	3.3
2/15	2.9
3/15	2.2
4/15	2.0
5/15	1.7
6/15	1.5
7/15	1.4
8/15	1.4
9/15	1.4
10/15	1.3
11/15	1.3
12/15	1.2
13/15	1.2
14/15	1.1
15/15	1.1
Fraction of BWR Rods	**Peak Strain (%)**
1/7	1.1
2/7	1.0
3/7	0.85
4/7	0.83
5/7	0.78
6/7	0.66
7/7	0.62

by a 100-G side impact. Table 8 gives the peak rigid-body accelerations for each of the analyses. The rod was then assumed to fail whenever a scaled strain level anywhere along the length of the rod equals or exceeds the strain failure criterion.

Use of extrapolated amounts of future discharges of intermediate and high burn-up fuel with the 1994 data for metric tons of spent fuel by burn-up range produces the basis for constructing an average strain failure criterion as a weighted sum of strain failure levels weighted by the amount of spent fuel in each burn-up range. To do this, the cladding strains that produce rod failure are assumed to increase roughly linearly with decreasing fuel burn-up. High burn-up (55 to 60 GWDt/MTU) spent fuel is assumed to fail at 1 percent strain, intermediate burn-up (40 to 45 GWDt/MTU) spent fuel fails at 4 percent strain, and low burn-up (0 to 25 GWDt/MTU) spent fuel fails at 8 percent strain. Weighted summation of these cladding strain levels by burn-up range produces an average failure stain level of 3.6 percent. This average is probably somewhat low for three reasons: (a) because it is derived using uniform elongation strains which are expected to underestimate somewhat the strains required to produce rod failure, (b) because not all operating reactors will extend their operating life to 40 years, and (c) because not all operating reactors will convert to a fuel management cycle that produces high burn-up fuel.

Table 8 - Peak Accelerations from Rigid Target Impacts without Impact Limiters for the Monolithic Steel Rail Cask, Gs

Orientation	30 mph	60 mph	90 mph	120 mph
Corner	93.8	174.2	259.1	335.1
End	169.8	424.4	513.8	580.8
Side	98.3	241.3	424.4	491.5

References

[1] J. L. Sprung et al., "Reexamination of Spent Fuel Shipment Risk Estimates," NUREG/CR-6672, U.S. Nuclear Regulatory Commission, Washington, DC, March 2000.

[2] J. A. Koski, D. J. Ammerman, and R. J. Dukart, "NUREG/CR-6672: Generic Casks and their Response to Fires", Proceedings, PATRAM 2001, Chicago, IL, USA, Sept. 2001.

[3] J. L. Sprung, "NUREG/CR-6672: Accident Severity and Release Fractions", Proceedings, PATRAM 2001, Chicago, IL, USA, Sept. 2001.

[4] L. M. Taylor and D. P. Flanagan, "PRONTO 3D, A Three-Dimensional Transient Solid Dynamics Program," SAND87-1912, Sandia National Laboratories, Albuquerque, NM, March 1989.

[5] S. W. Attaway, "Update of PRONTO 2D and PRONTO 3D Transient Solid Dynamics Program," SAND90-0102, Sandia National Laboratories, Albuquerque, NM, November 1990.

[6] V. L. Bergmann, "Transient Dynamics Analysis of Plates and Shells with PRONTO 3D," SAND91-1182, Sandia National Laboratories, Albuquerque, NM, September 1991.

[7] American Society of Mechanical Engineers, "Specification for Alloy-Steel Bolting Materials for Special Applications," SA-540, ASME, New York, NY, 1998.

[8] Parker Seal Group, "Parker O-Ring Handbook," Parker Hannifin Corporation, Cleveland, OH, 1992, pp. A4-7.

[9] A. Gonzales, "Target Effects on Package Response: An Experimental and Analytical Evaluation," SAND86-2275, Sandia National Laboratories, Albuquerque, NM, May 1987.

[10] I. G. Waddoups, "Air Drop Test of Shielded Radioactive Material Containers," SAND75-0276, Sandia National Laboratories, Albuquerque, NM, September 1975.

[11] L. L. Bonzon and J. T. Schaumann, "Container Damage Correlation with Impact Velocity and Target Hardness," IAEA-SR-10/21, Transport Packaging for Radioactive Materials, IAEA, Vienna, Austria, 1976.

[12] T. L. Sanders, et al., "A Method for Determining the Spent-Fuel Contribution to Transport Cask Containment Requirements," SAND90-2406, Sandia National Laboratories, Albuquerque, NM, November 1992.